# Spatial distribution of atomic electronic density for elements 1 to 54 as coming from a Hartree-Fock treatment within the minimum atomic parameters (MAP) paradigm.

Peter Reinhardt, Ilya Popov, Andrei L Tchougréeff

# Spatial distribution of atomic electronic density for elements 1 to 54 as coming from a Hartree-Fock treatment within the minimum atomic parameters (MAP) paradigm.

Peter Reinhardt[1], Ilya Popov[2], Andrei L. Tchougréeff[2,3]

[1]*Laboratoire de Chimie Théorique, Sorbonne Université et CNRS UMR7616, Paris, France; email:* Peter.Reinhardt@Sorbonne-Universite.fr

[2]*Frumkin Institute of Physical Chemistry and Electrochemistry, Russian Academy of Sciences, Moscow, Russia*

[3]*Institut für Anorganische Chemie, RWTH Aachen, Aachen, Germany*

## Abstract

The minimum atomic parameters/Moscow-Aachen-Paris (MAP) basis sets — reintroduced in the previous paper[1] — are analyzed with respect to spatial features as orbital shape, possible fits to alternative orbital sets (numerical or quasi-numerical orbitals, nodeless Slater orbitals), respect of Kato's condition and radial distribution of energy components.

For comparing orbital spaces the Frobenius angle between the orbital subspaces they span is introduced as numerical tool. It is shown that the electronic density of the MAP states is depleted around the nucleus with respect to the other orbital sets. Despite this, the similarity between the respective subspaces in all cases (except a unique case of the Pd atom) as measured by the cosine of the Frobenius angle amounts above 0.96 for all atoms. Deviations from the perfect value of Kato's condition amounts systematically to 0.3 and 0.5 for all elements considered. Integrating one-electron energy contributions from $r = \infty$ to a finite radius, MAP and Bunge orbitals show about the same values, but for the inner region governed by the polynomial oscillations.

**Contents**

## I. INTRODUCTION. RECALL OF THE MAP ORBITALS

In the previous paper,[1] hereafter referred to as I, we extend the analysis of atomic orbitals constructed via a minimal-parameter procedure, specifying only one single exponent per subshell. This procedure – reintroduced in Ref. 2 for the atoms of the 2$^{\text{nd}}$ period – actualizes the original idea dating back to 1930ies.[3]

In this setting the orthogonality of the atomic functions is obtained by writing the radial function $R_{n\ell}(r)$ as a polynomial of order $(n-1)$ in $r$ times an exponential function $\exp(-\xi_{n\ell}\, r)$ and by solving hierarchially the orthonormality conditions for so-constructed functions within a set of common $\ell$. Orbital exponents $\xi_{n\ell}$ are chosen to minimize the total energy[4–6] for a given electron configuration, leading to a restricted open-shell Hartree-Fock procedure.

As we have shown in paper I, such a setting misses about 3 % in total energy with respect to numerical Hartree-Fock orbitals,[7,8] or expansions in the large Slater-type basis sets of Bunge et al.,[9] which in their turn give the results at $\mu$-Hartree precision with respect to the previous. Despite this loss in total energy with respect to purely numerical, basis-set-free Hartree calculations, MAP orbitals have an overlap with their numerical analogues of more than 90 %.

As for physical properties, the periodicity of Mendeleev's Table is well reproduced by the MAP orbitals in terms of atom sizes. A remarkable feature of the MAP orbitals is that the positions of the nodes in the individual orbitals of a given atom and given angular quantum number $\ell$ almost coincide for different allowed values of the principal quantum number $n\,(\ell \geq n-1)$ with the coincidence being particularly close for the innermost nodes.

In the present manuscript we investigate further the connections between MAP orbitals and the two other extremes, numerical orbitals on one side and nodeless Slater orbitals on the other, by looking at orbital shapes, mutual fits of parameters, radial integration and Kato's condition as test. Conclusions from these and an outlook to potentially interesting applications close this contribution.

Purely technical details are collected in an Appendix, and a compilation of the data can be found in the accompanying Supplementary Material. The underlying MAP orbital exponents are found in the Supplementary Material of paper I.[1]

## II. DISCUSSION

All data of this manuscript refer to the electronic ground states of the respective chemical elements, as given by the Madelung-Klechkowski rule (or *Aufbau* principle).[10,11] Known exceptions to this rule like Cr, Cu, Pd etc will be discussed in a forthcoming paper, together with a more detailed look at excited states in general.

### A. Orbital shapes

Obtained orbitals in the minimal-parameter set may be inspected and compared to available (quasi-)numerical Hartree-Fock orbitals.[7,9] We observe as general aspect that while the long-range tail is comparable in both orbital sets, the region close to the nucleus manifests significant differences. Specifically, despite the correspondence of the positions of the radial nodes of both the Bunge and MAP functions, the amplitudes of the oscillations of the MAP orbitals coming from the polynomial multiplier are much less pronounced than for Bunge orbitals, especially when comparing valence orbitals, see Figure 1.

Of course, orthonormality imposes the nodal structure of the orbitals, even if the population inside the outermost node, i.e. the integral of the squared orbital from zero to the position of this node, does not exceed some percent of the total population of the orbital. This led already Slater to simplify radial functions toward nodeless orbitals,[12,13] and as well for orbitals suited for pseudopotentials the nodal structure is entirely ignored.[14–17] In the latter case it had been shown that even if Hartree-Fock valence energies are well reproduced, the absence of the inner nodal structure induces significant errors when calculating valence correlation energies. Since presently we concentrate on the features of the Hartree-Fock based MAP states we postpone the discussion of this issue for the future.

Plotting the inner population for MAP and Bunge orbitals as shown in Figure 2 reveals that the spatial distribution of electron density is not the same within the two orbital sets. The difference is relatively small for $2s$ orbitals, but it becomes quite pronounced for higher $n$. Systematic differences can be seen as well for the series of transition elements ($Z = 21 - 30,\ 39 - 48$), where the $4s$ and, correspondingly, the $5s$ inner population for numerical orbitals – a few percent of the total orbital population – decreases with increasing $Z$, but is hardly detectable for MAP orbitals for these elements.

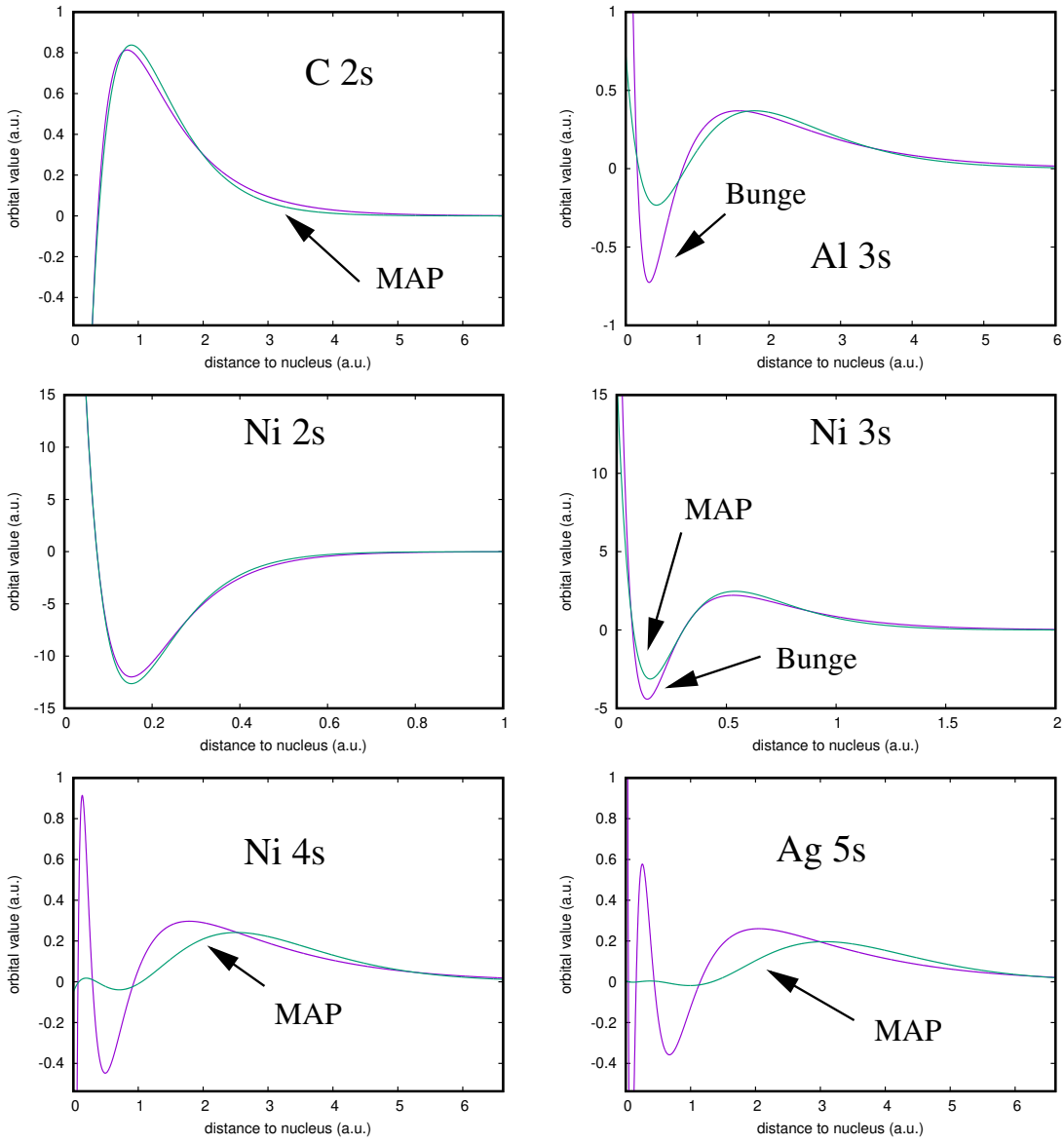


FIG. 1: Illustrating the previous findings at hand of the spatial extension of the $n$s valence orbitals of C, Al, Ni and Ag. Despite significant differences in the vicinity of the nucleus, the overlap $\int_0^\infty R_{\mathrm{Bunge}}(r) R_{\mathrm{MAP}}(r)\, r^2\, dr$ of the corresponding functions is always larger than 90 %.

As we reported in paper I, total energy and atomic radius are affected only weakly by these differences of density distributions, so that overlaps between MAP and Bunge orbitals remain within 95 %.

Comparing orbitals in two basis sets one by one does not provide an integral picture. Fundamentally, we should compare functional *subspaces* spanned by the two basis sets. This can be easily done with help of the Frobenius inner product of the projection operators

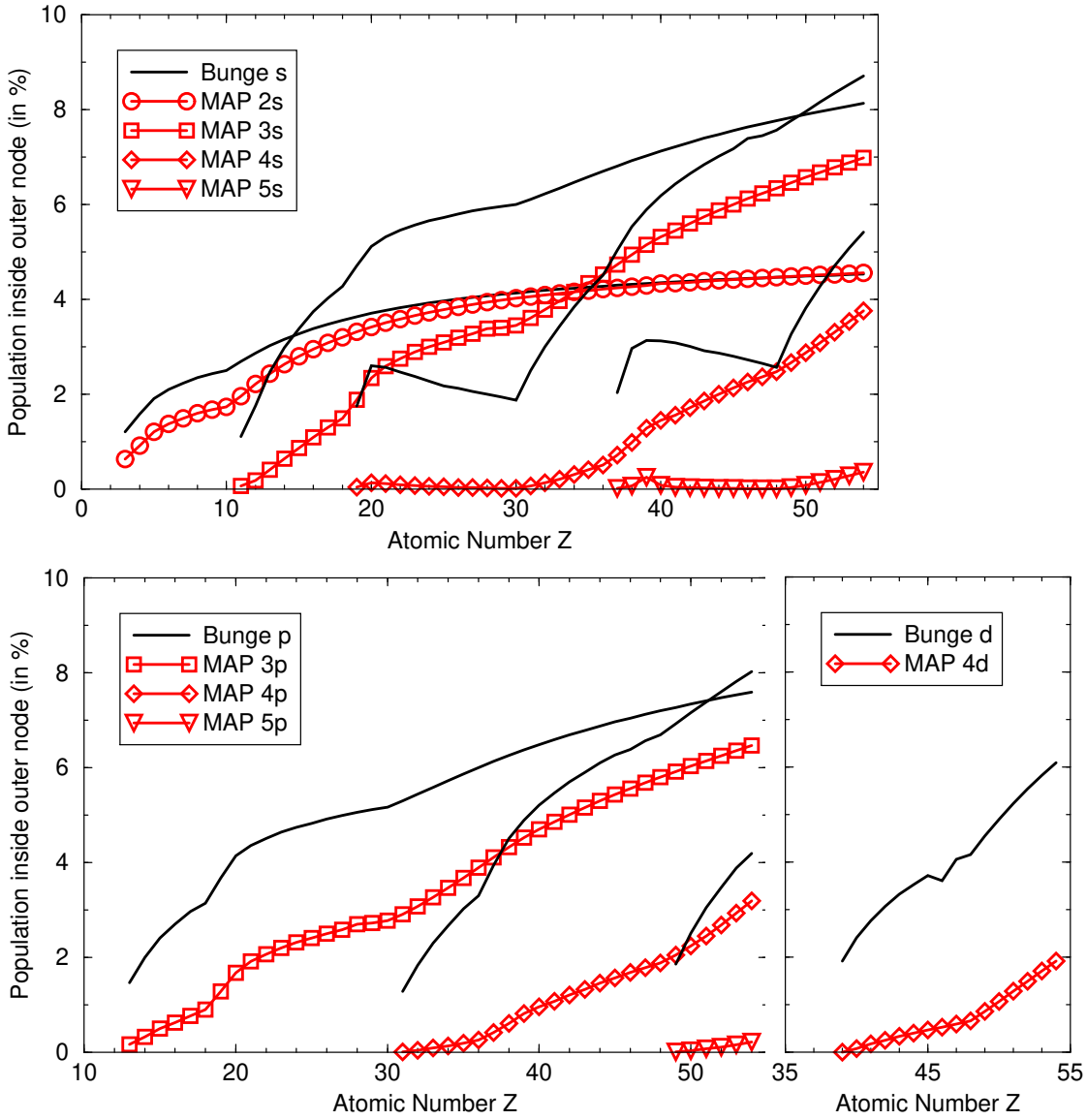


FIG. 2: Integration of the radial density up to the outermost node, for Bunge orbitals, and for the corresponding MAP orbitals. Upper panel shows the 2s to 5s, starting at Z=3, 11, 19, and 37, respectively. Left lower panel displays the $p$ series, starting, respectively, at Z=13, 31 and 49. The 4d orbitals are shown in lower right panel.

on the respective subspaces (for details see Appendix III A) as a numerical tool. Physically, the cosine of the angle between the subspaces as defined by eq. (4) gives the probability for a particle (electron) abiding in a state belonging to one subspace to occur in a state of another one.

Figure 3 shows that the so-defined probability remains of the order of 95 % throughout

the whole range of elements of the Periodic Table covered here. We observe two exceptions: the optimization of orbital exponents leads to a very small 4d exponent (0.636) for Yttrium ($Z = 39$), and for Pd ($Z = 46$) we optimized exponents for a $4d^8 5s^2$ high-spin state instead of the physical $4d^{10} 5s^0$ ground state.

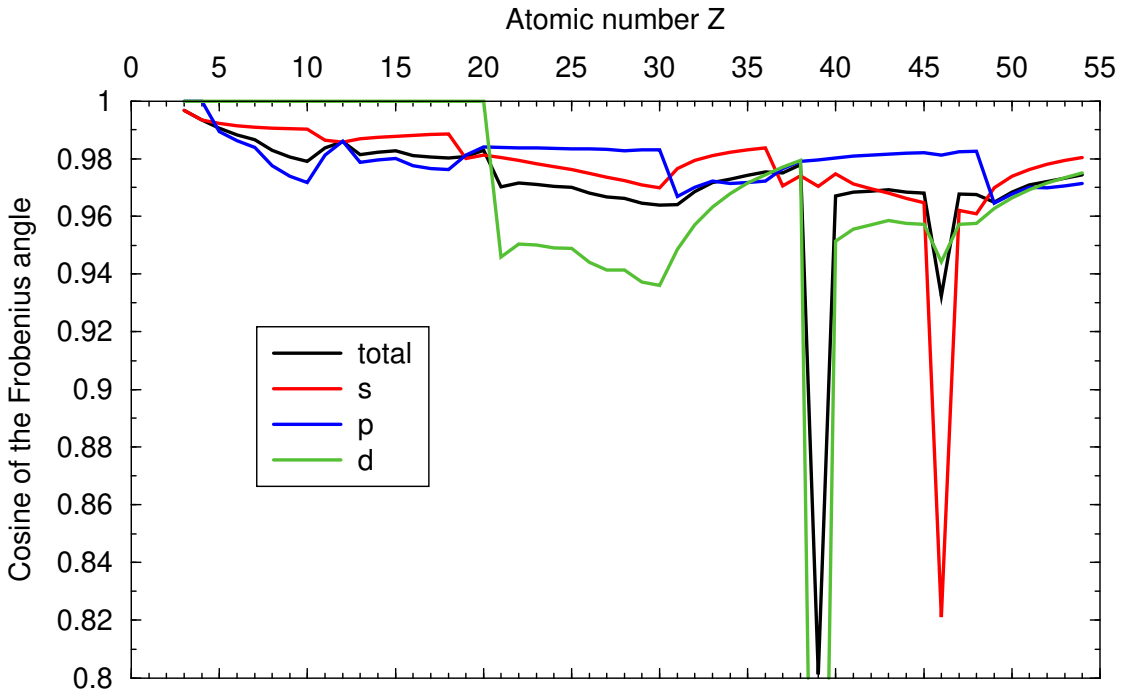


FIG. 3: The cosine of the Frobenius angle eq. (4) between the subspaces given by Bunge and MAP orbitals. The two exceptions are the 4d orbital of Yttrium ($Z = 39$), and the 5s orbital of Palladium ($Z = 46$).

### B. Mutual fitting of orbital sets

While numerical Hartree-Fock orbitals can be considered as parameter-free (making abstraction of the radial integration points), we may introduce several different optimization criteria for the parameters defining either MAP or nodeless Slater orbitals.

#### 1. *Orbital optimization with nodes fixed at the positions of the nodes given by numerical orbitals*

Having observed that the orbital shapes in the core region are significantly different between the MAP and Bunge/numerical orbitals, despite the relative smallness of the total-

energy differences and large overlaps, we may have a closer look to the nodes of the orbitals. As we could see for the Iodine $5s$ orbital as example (see Figure 5 of paper I), the nodes are nearly coinciding, although not identical between the MAP and Bunge's orbitals.

The numerical orbital has, due to the orthogonality constraints, as many nodes as our orbitals. We may try to fit thus the MAP expression to this orbital, going through exactly the same nodes. Before doing so, we divide numerically the radial function of numerical orbitals by the corresponding polynomial factor. As shown in Figure 4, the ideally linear relations are well visible for the inner shells, and as well the shell structure is clearly reproduced.

Fitting a MAP orbital to the corresponding numerical Hartree-Fock or to Bunge orbital comes then down to a linear regression with the slope (i.e. the MAP exponent) as only free parameter. The intercept is fixed through the normalization condition.

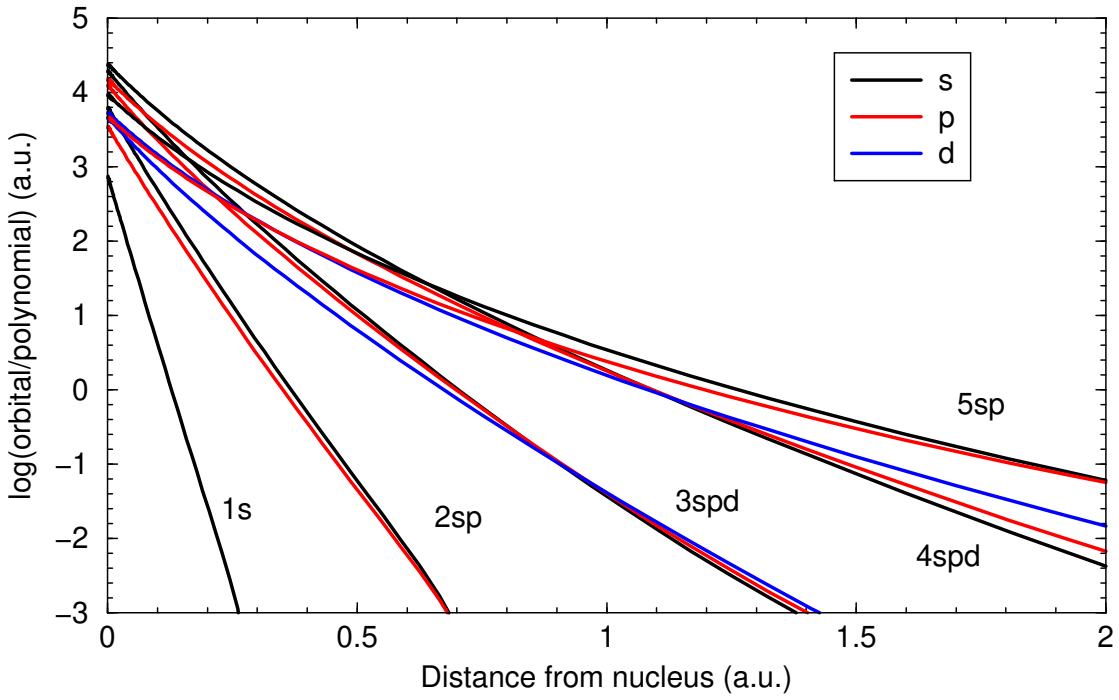


FIG. 4: For Iodine we show the numerical Hartree-Fock orbitals – as obtained by the Froese-Fischer program[7] – divided by the polynomial fixed by the orbital nodes, in a logarithmic scale. The $1s$ orbital is a pure exponential function; however the deviations from the ideal relations are more and more pronounced for increasing $n$.

Optimizing the overlap of the Bunge and MAP states while keeping the node positions fixed at those of Bunge's orbitals gives for instance the Iodine $5s$ orbitals an exponent of

3.18631 with overlap of 0.964, almost identical with one found via the energy optimization in the MAP setting: 3.1897. A more detailed compilation of the results of the described procedure applied to the whole set of Iodine orbitals is given in Table I.

TABLE I: MAP exponents for an Iodine atom. The first column gives the previously obtained MAP exponents (see Suplementary Material of paper I for full-precision data), second column gives the overlap (in per cent) of the MAP function and a corresponding nodeless Slater orbital $r^{(n-1)}e^{-\xi r}$. Third and fourth column show the data for the exponents obtained by maximizing the overlap of the same $n\ell$, respecting norm and positions of the nodes. Total energies are (in Hartree) $-6917.981$, $-6893.773$, $-6881.287$ for Bunge, variational MAP, and the present fit, respectively. For calculating a total energy from the fitted exponents, orbitals were re-orthogonalized via the MAP construction. This shifts the node positions slightly, as Bunge nodes and orthogonality define too many constraints to be satisfied simultaneously within the minimal parameter space.

| Orb. | MAP exp. var. HF | MAP/Slater overlap | MAP exp. fitted to Bunge | maximized overlap in % |
|---|---|---|---|---|
| 1s | 52.686 | 100. | 52.3059 | 99.9993 |
| 2s | 25.249 | 87.8 | 24.2894 | 99.9565 |
| 3s | 14.883 | 72.1 | 13.8225 | 99.5837 |
| 4s | 8.1798 | 71.1 | 7.65756 | 98.3884 |
| 5s | 3.1897 | 86.4 | 3.18631 | 96.4233 |
| | | | | |
| 2p | 24.632 | 100. | 23.7707 | 99.9710 |
| 3p | 14.276 | 81.8 | 13.3155 | 99.5463 |
| 4p | 7.5596 | 77.5 | 7.05405 | 98.1482 |
| 5p | 2.7051 | 72.0 | 2.58773 | 95.9579 |
| | | | | |
| 3d | 12.988 | 100. | 12.1820 | 99.7152 |
| 4d | 6.1826 | 89.8 | 5.72662 | 97.5304 |

Taking the so-obtained, slightly non-orthongonal orbitals as starting point for our MAP energy optimization procedure we obtain again the previously generated, energy-minimizing exponents.

*2. Fit MAP to Bunge*

As mentioned in Section II A, the numerical measure of the coincidence between the orbital subspaces spanned by different basis sets is given by the Frobenius angle eq. (4) between them whose cosine is the probability of finding an electron in a subspace spanned by one basis set under the condition that it occurs in the subspace spanned by another one. We may thus use this quantity to fit MAP orbitals to Bunge orbitals without the exact node-matching.

Traditionally, (see *e.g.* 5,22–25) the quality of a fit is controlled by the achieved total energy as based on the variation principle. This approach is not, however, precisely what is needed. First, it requires the calculation of the energy which may be tedious. Second, in the strict sense, it produces the measure of the closeness of the specific (lowest energy) state approximations achievable in the subspaces rather than of the subspaces themselves. In the atomic context it means that in the energy-variation principle setting the states, say, in the valence subshell of an atom, are treated differently depending on the amount of electron population of the latter. Thus, the Frobenius angle or its cosine give a more uniform quantification of the similarity of the subspaces to be compared. An alternative set of MAP exponents can be obtained by maximizing the cosine of the Frobenius angle between the subspace spanned by the MAP states and the Bunge states. Resulting values of the cosine (probability) are plotted on Fig. 5.

and exponents are collected in Supplementary Materials. It is important to note that for the following five elements (Cu, Rb, Pd, Pt, Ag) values of so obtained 1s exponents exceed atomic numbers of the elements. The possible explanation is the presence in the respective Bunge basis sets of the STO primitives with exponents exceeding atomic number significantly contributing to the $1s$ orbitals.

*3. Fit of $Z_{\text{eff}}$ of the Slater model to MAP and Bunge orbitals*

The Frobenius scalar product allows to quantify the difference between different orbital sets. Another measure may be to fit a well-defined third orbital class to either set, for instance Slater's nodeless radial functions, by maximizing the overlap between the orbital sets.

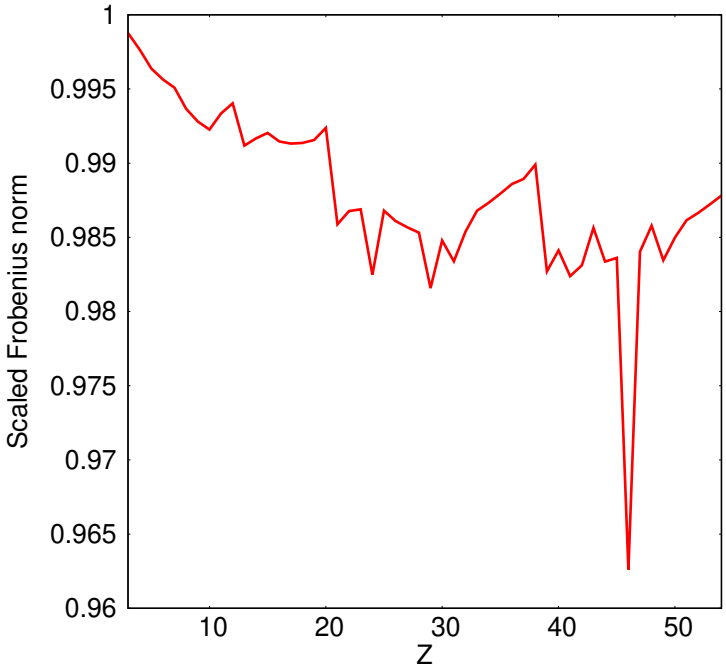


FIG. 5: Optimized cosine of the Frobenius angle between subspaces spanned by MAP and Bunge sets against atomic number. Resulting probabilities (cosine of the Frobenius angle) exceed 0.98 for all atoms except Pd, where its value nevertheless remains 0.96.

Again, we have just one single parameter per subshell, as all others are fixed. Slater proposed in his landmark paper[13] a simple estimation of screening constants $\sigma$ when writing radial funcions as

$$R_{n^*}(r) = N_{n^*} r^{(n^*-1)} e^{-(Z^*/n^*)r} \qquad \text{with} \qquad Z^* = Z - \sigma$$

For $n > 3$ the effective $n^*$ is proposed to be set to values different from $n$, i.e. 3.7 instead of 4, and 4 instead of 5 (for our ensemble of elements up to $Z = 54$).

The overlap of a MAP or Bunge orbital with a primitive Slater orbital may be easily calculated as a function of $Z^*$ with the help of Mathematica,[18] and incorporated in an optimization procedure.

For the iodine atom as example we find the best $Z^*$ yielding the maximal overlaps as given in Table II.

We see immediately that overlaps between MAP and Bunge states are always better than 0.95, and the obtained $Z^*$ are very close. However, the resulting $2s$ exponent is considerably smaller than the $2p$ exponent, and the same holds for the $3p$ exponent. For these two

TABLE II: Slater's effective nuclear charges $Z^*$ and maximized overlaps and corresponding $Z^*$ for MAP/Bunge orbitals and Slater orbitals $r^{(n^*-1)}\exp(Z^*/n^*\,r)$, for the iodine atom, $Z = 53$. We give in the last column also the overlap between the MAP and Bunge orbital for sake of completeness.

| Orb. | Slater's | MAP | | Bunge | | |
|---|---|---|---|---|---|---|
| | screened $Z^*$ | max. Overlap | $Z^*$ | max. Overlap | $Z^*$ | $S_{\mathrm{MAP/Bunge}}$ |
| $1s$ | 52.69 | 1.000000 | 52.6862 | 0.999993 | 52.3059 | 0.999973 |
| $2s$ | 48.85 | 0.932635 | 38.8031 | 0.938749 | 37.3943 | 0.998507 |
| $3s$ | 41.75 | 0.882507 | 30.8542 | 0.895175 | 28.4649 | 0.989460 |
| $4s$ | 25.25 | 0.896528 | 19.6500 | 0.893065 | 17.8801 | 0.977660 |
| $5s$ | 7.60 | 0.947849 | 8.13347 | 0.942856 | 7.97763 | 0.958939 |
| $2p$ | 48.85 | 1.000000 | 49.2630 | 0.999710 | 47.5415 | 0.998949 |
| $3p$ | 41.75 | 0.910455 | 32.2099 | 0.919719 | 29.7338 | 0.990418 |
| $4p$ | 25.25 | 0.914354 | 18.9800 | 0.911075 | 17.2700 | 0.976573 |
| $5p$ | 7.60 | 0.958761 | 7.13512 | 0.959876 | 6.82707 | 0.954011 |
| $3d$ | 31.85 | 1.000000 | 38.9644 | 0.997152 | 36.5458 | 0.993981 |
| $4d$ | 13.85 | 0.953058 | 17.2792 | 0.948578 | 15.8040 | 0.972777 |

orbitals the relatively large oscillations of the polynomial render the best-overlap nodeless Slater functions shifted with respect to the main lobes. A larger exponent would fit the outer region better, but gives a smaller overlap in the inner region. For the higher-$n$ orbitals this is less important as the polynomial oscillations are weaker, and thus the common decay at larger distances is more significant for the best overlap. Of course, this is only a rough argument for comparing these qualitatively different orbital sets.

Looking at Table 2 and Figure 2 of paper I and the Figure 8 showing the trends in the exponents for different subshells with $Z$, one immediately observes a striking precision with which the slopes for the exponents of the four deepest shells ($n = 1 \div 4$) follow the $Z/n$ trend. However, a closer look to the supposed linear relations of the exponents with respect to $Z$ reveals systematical deviations, depicted in Figure 7 which cannot be imputed to numerical instabilities.

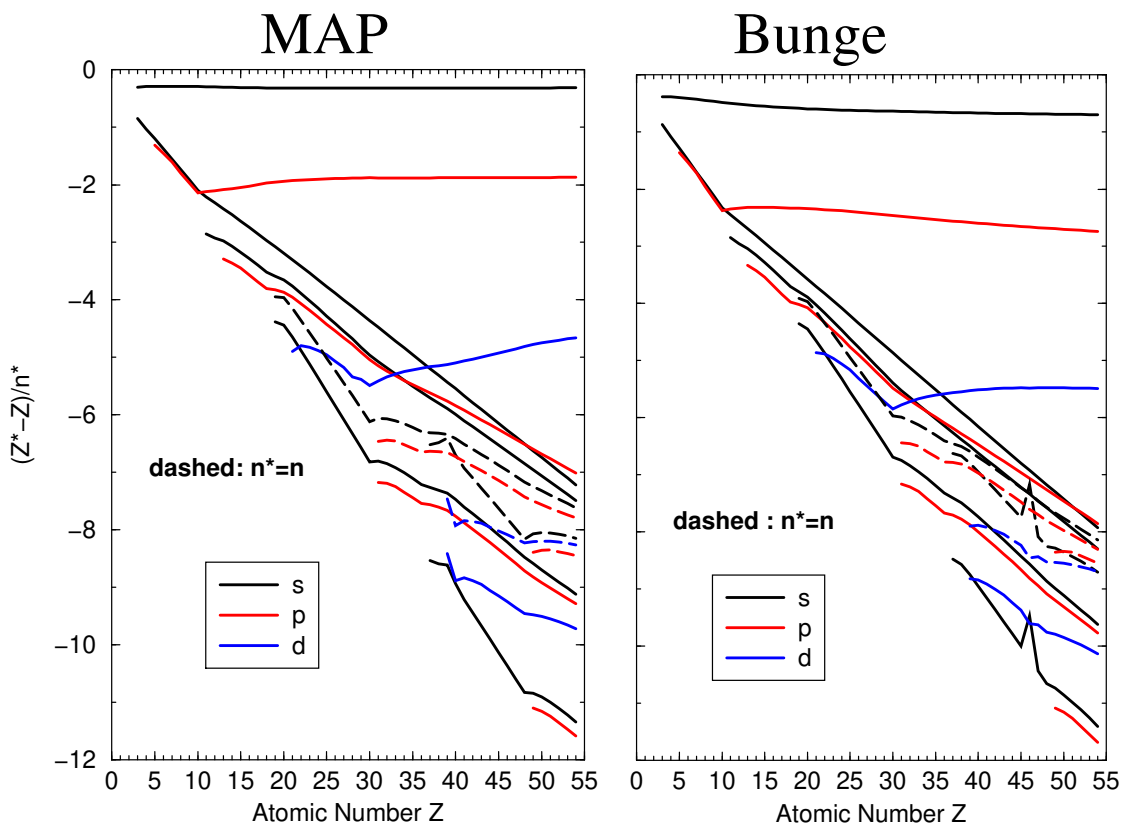


FIG. 6: Effective diminuation of the orbital exponent due to screening of the nucleus ($\frac{Z-Z^*}{n^*} = -\frac{\sigma}{n^*}$) for Slater exponents fitted to MAP orbitals (left panel) and Bunge orbitals (right panel). Shells can be identified from the starting points of the lines. The spike in the rhs panel is Pd (Z=46).

For the shell with $n = 5$ the deviation from this trend is quite pronounced which may be considered as a hint towards the effective principal quantum numbers $n^*$ introduced by Slater.[13] The inverse of the coefficients $a$ for the $5s$ and $5p$, respectively, equal to 3.717 and 3.875. On the other hand one needs to recollect the interpolation used by Slater for the orbital exponents:

$$\xi_{n\ell} = \frac{Z - \sigma_{n\ell}(Z)}{n^*}, \tag{1}$$

which contains – in counterpoise to somewhat reduced values of the effective principal quantum number ($n^* \leq n$) – the screening constants $\sigma_{n\ell}(Z)$ as well.

We may, of course, introduce the same constraint of common $sp$ exponents in our optimization procedure. When plotting the deviations from $Z/n$ for the first three principal numbers, the coincidence of the simple Slater model and our MAP basis sets is as well strik-

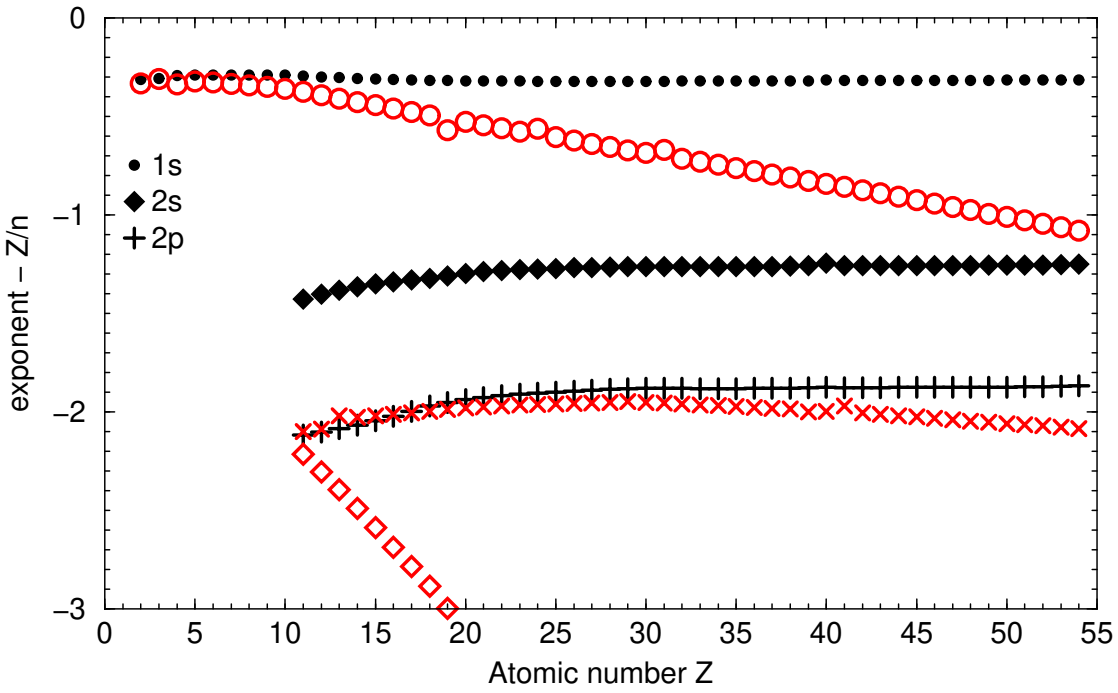


FIG. 7: Deviation from the linear relation $\xi = Z/n + c$, for our basis sets (black symbols) and for the single-$\zeta$ basis sets of Clementi and Raimondi (red symbols). We take only $n = 1$ (rounds) and 2s (diamonds), 2p (crosses) as non-valence shells.

ing. As for saturated subshells the screening in the Slater model becomes a constant and thus $(Z^*/n) - (Z/n)$ (or using $n^*$ for $n > 3$).

For the $1s$ orbital this is the same for MAP orbitals, and nearly so for the $2s$ orbital. But from $2sp$ on this is not any more the case, the $2p$ orbital exponent plotted in Fig. 8 follows right from the beginning a different slope, and the screening saturates only around $Z = 25$. Again this is coherent with the discussions on small- and large-core effective core potentials for transition elements. Forcing a common exponent for $2s$ and $2p$ (red curves in Figure 8) indicates that the trend characteristic for $s$ orbital prevails over that for the $p$ orbital. And for $n = 3$ we cannot speak any more of a constant screening, at least not for the first 54 elements. The presence of $3d$ electrons perturbs the strictly hierarchical order with Slater's model, leading as well to significant differences for the $3d$ orbital exponents.

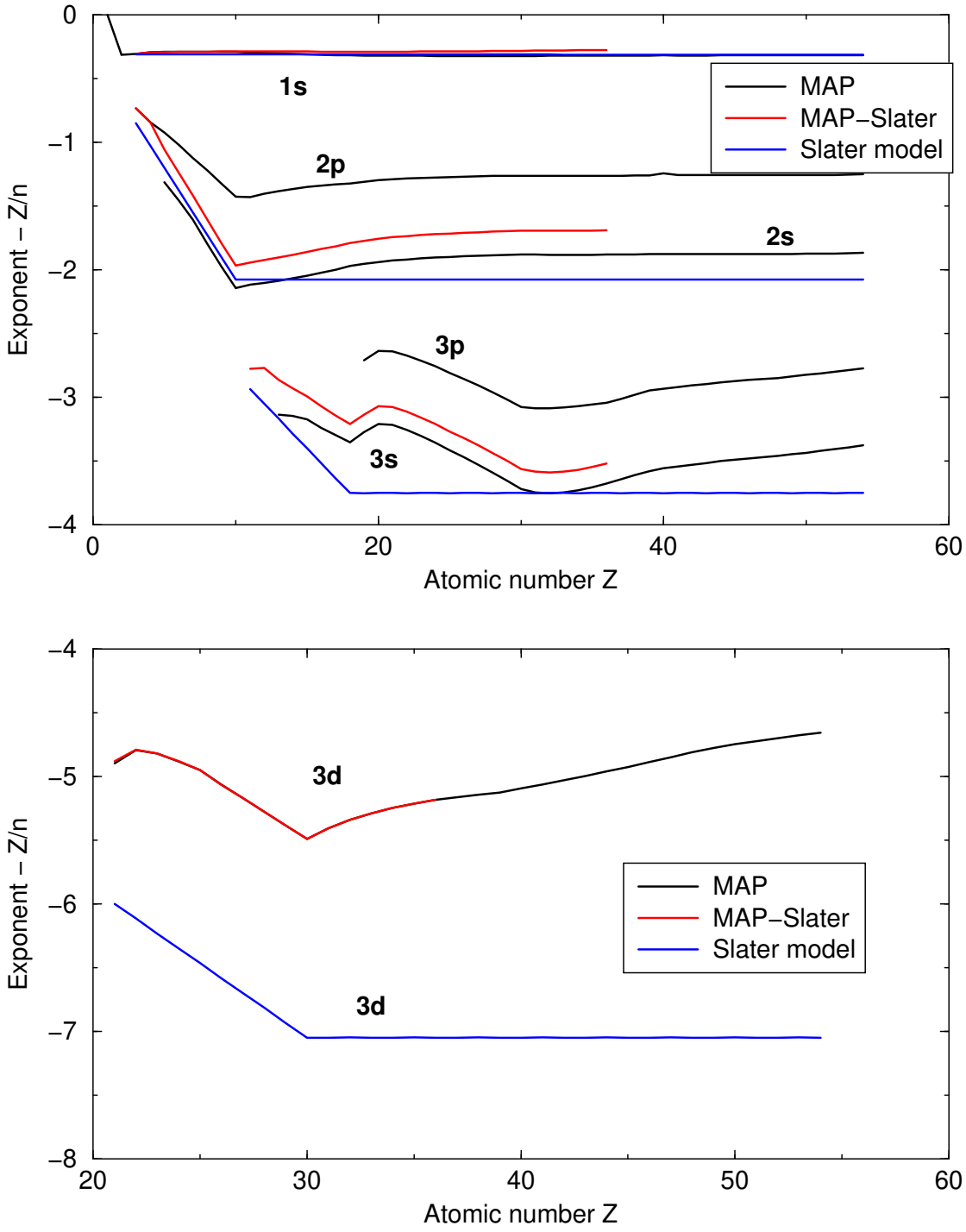


FIG. 8: Comparison of MAP basis sets, optimization with common *sp* exponents and the simple Slater model of 1930. The screening constants in the latter do not evolve once the considered shell becomes an inner one.

TABLE III: Data obtained from the fit parameters $a$ and $b$ of Table 2 of paper I. We obtain similar parameters as proposed by Slater in 1930 for an effective principal number $n^*$ and a screening constant corresponding roughly to the number of inner electrons for each shell.

| Orbital | character | $Z$-range | $1/a$ | $-n^*b$ | "$N_{\mathrm{core}}$" |
|---|---|---|---|---|---|
| $1s$ | core | 3–54 | 1.00 | 0.28 | 0 |
| $2s$ | core | 5–54 | 1.98 | 2.82 | 2 |
| $2p$ | core | 11–54 | 1.98 | 2.82 | 2 |
| $3s$ | core | 13–54 | 2.98 | 8.76 | 10 |
| $3p$ | core | 19–54 | 3.01 | 10.41 | 10 |
| $3d$ | core | 31–54 | 2.73 | 19.26 | 18 |
| $4s$ | core | 37–54 | 3.89 | 20.35 | 28 |
| $4s$ | non-transition | 31–36 | 3.25 | 27.86 | 30 |
| $5s$ | non-transition | 49–54 | 3.72 | 44. | 46 |
| $2s$ | valence | 3–4 | 2.49 | 0.88 | 2 |
| $2p$ | valence | 5–10 | 3.01 | 0.9 | 2 |
| $3s$ | valence | 11–12 | 3.05 | 7.89 | 10 |
| $3p$ | valence | 13–18 | 3.47 | 7.56 | 10 |
| $3d$ | valence | 21–30 | 3.82 | 9.69 | 10 |
| $4s$ | "valence" | 19–20 | 3.19 | 18.53 | 18 |
| $4d$ | valence | 39–48 | 3.63 | 31.60 | 36 |
| $5s$ | "valence" | 37–38 | 3.56 | 37.48 | 36 |
| $5p$ | valence | 49–54 | 4.30 | 37,88 | 48 |
| $4s$ | transition | 21–30 | – | – | |
| $5s$ | transition | 39–48 | – | – | |

### C. Kato's condition

As commonly known, the exact electron density must have a cusp at the nuclear position, respecting Kato's condition:[19]

$$\frac{1}{2}\frac{|\vec{\nabla}\rho(\vec{r})|_{\mathrm{sph.\,av.}}}{\rho(\vec{r})}\bigg|_{r=0} = Z. \tag{2}$$

Taking numerical Hartree-Fock orbitals or Bunge's basis sets we see that this condition is fulfilled already at the Hartree-Fock level,[8] and even individually for each atomic $s$ orbital[20] — the only ones with a non-vanishing electron density at the origin.

Despite the sizable absolute deviation of the gradient-to-density ratio from the ideal value of $Z$ it does not show any significant or characteristic variation with $Z$, ranging from 0.3 for a helium atom to around 0.5 for the heavier elements. The relative deviation (that divided by $Z$) fades out with increase of $Z$. Electron correlation as missing ingredient in the Hartree-Fock approach can be ruled out being responsible for this deviation as the electron density and orbitals within Bunge's basis sets reproduce correctly the nuclear cusp.

We find that the $1s$ exponent alone dictates the value of the gradient at the origin. The other $s$ orbitals change this quantity only very little, as they add in a similar way to the numerator and the denominator of the expression. For instance for the Sulfur atom ($Z = 16$) we find as individual $|\vec{\nabla}\rho(\vec{r})| \,/\, \rho(\vec{r})\Big|_{r=0}$ values of 15.6886, 14.1127 and 11.1905 for 1s, 2s, and 3s, respectively, leading as a sum to 15.6052. Using Bunge's basis sets the corresponding data are 15.9999, 15.9919 and 15.9976 with a sum of 15.9993, very close to the expected result.

The overall results, as cumulative sums in numerator and denominator of the reduced density gradient, are depicted in Figure 9; the smooth curves allow an estimation of the numerical noise of our multi-parameter optimization procedure.

We see as well that the $4s$ and the $5s$ orbitals do not add any change to the cumulative sums. This is due to the very low electron density a the origin, for instance for the I atom in the MAP setting we have densities of 7499, 757.5, 99.83, 3.100, and 0.001045 (in atomic units) for 1s to 5s, respectively. For orbitals expanded in the Bunge basis set, the figures read 7391, 779.5, 154.7, 31.45 and 3.639, reflecting the same findings as for the populations inside the polynomial region.

### D. Radial integration of one-electron quantities

Kato's condition "measures" the orbitals in the vicinity of the nucleus. For looking at the opposite side, we may integrate energy contributions[8] from outside toward the nucleus, like kinetic energy or the electron-nucleus attraction. In this way we see, in which region the difference in total energy between the MAP and the Bunge orbital sets are located.

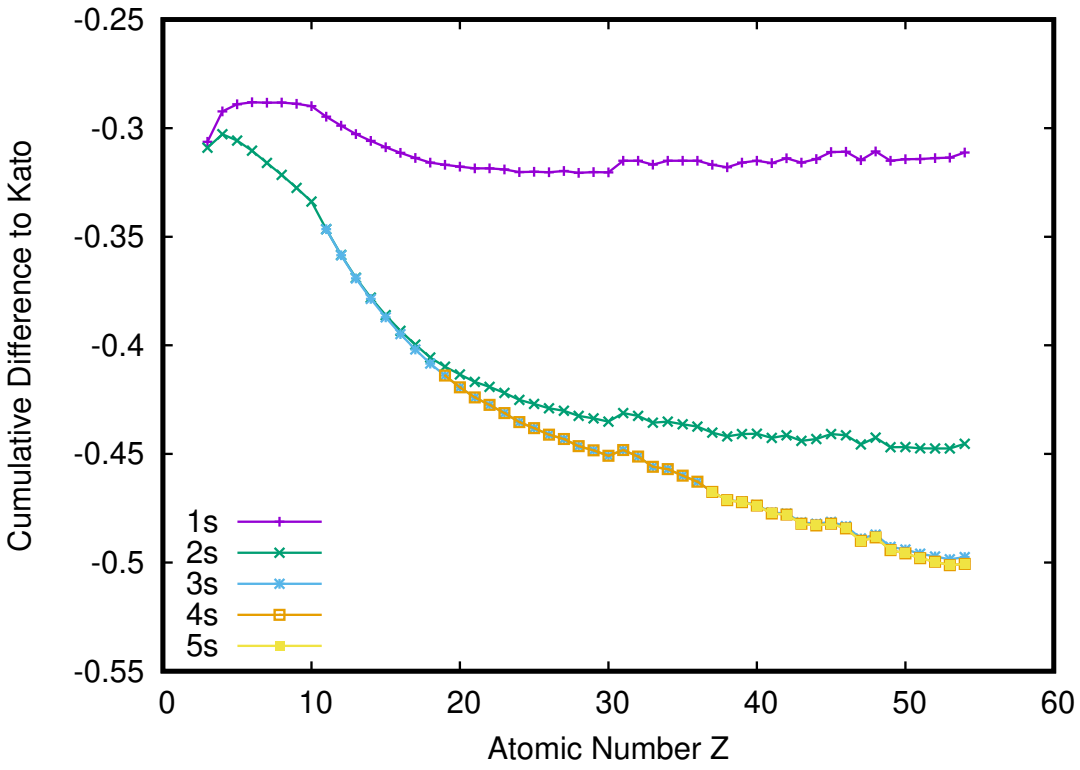


FIG. 9: Deviation from Kato's condition $(1/2)\,|\nabla\rho|/\rho - Z \;=\; 0$ at the nucleus, evaluated directly from the radial functions of the $s$ orbitals.

Figure 10 shows these contribtions for the orbitals already displayed in Figure 1. If for the carbon $2s$ orbital the difference is hardly visible, we see for the Ni $4s$ and Ag $5s$ orbital the kinetic-energy contributions to the total energy are not systematically underestimated by the MAP orbitals,

Radii for the shown elements (C, Al, Ni, Ag) are 1.94025, 3.34261, 3.20627 and 3.63247 Bohr, respectively, and nodes of Bunge orbitals are situated at 0.376 a.u. (C, $2s$), 0.797 and 0.162 (Al, $3s$), at 0.0742 (Ni $2s$), 0.304 and 0.0718 (Ni, $3s$), 0.936, 0.296 and 0.0716 (Ni, $4s$), and, finally, at 1.149, 0.439, 0.162, and 0.0417 a.u. (Ag, $5s$). We marked these in the plot.

In the region outside the atomic radius the two orbital sets are close, and significant deviations for the radial integration occur only within the nodal region, too close to the nucleus with respect to the chemically important valence region. We can thus expect that atoms described with MAP orbitals will produce chemically relevant data, without the need for long basis set expansions. The density missing in the core region is distributed in a wide range in the outer orbital lobes, rendering them only insignificantly different to numerical

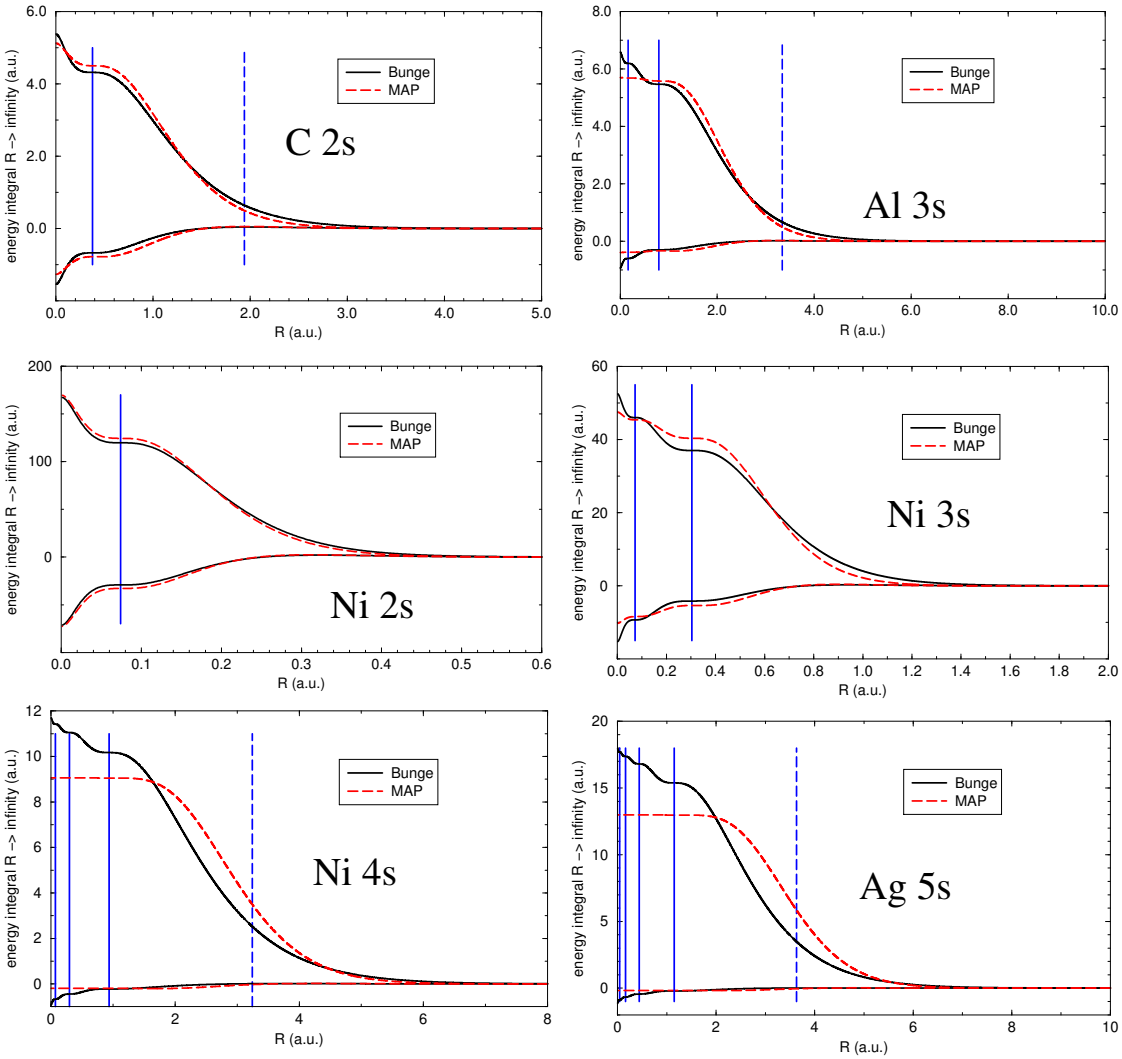


FIG. 10: The integral from $R$ to $\infty$ of the kinetic energy (positive) and e-n one-electron contribution to the potential energy (negative), for the six orbitals of Figure 1. We mark as vertical lines the positions of the orbital nodes, and for the valence orbitals with a broken vertical line the atomic radius.

or high-precision orbitals, be it in Gaussian or Slater expansions. The former are not well suited close to the nucleus or far away, however, in the intermediate region to which we are focussed, they are as well suited.

### E. Relation to the general basis-construction problems

Depending on the application, a typical ab initio Gaussian basis set employs 10–200 GTO functions per atom, optimized with some criterion but without whatever individual meaning.[20] Yet at pretty early stage there were attempts to reduce the number of independent parameters in so-constructed sets by subjecting the exponents of the *Gaussians* to some parametric form. After the STO-nG series,[21] this gave rise to well-tempered and even-tempered basis sets,[22–25] well known in the literature. Remarkably, the functions of these sets have been obtained by minimizing the total energy in the Hartree-Fock approximation by which basis sets eventually spanning the same subspace as the Bunge basis sets, the latter very close to numerical Hartree-Fock orbitals obtained on radial grids.[7] The parameters used for the construction of even- or well-tempered exponent sequences, universal[22,24] or atom-specific,[25] do not have any meaning by themselves – they are merely numbers.

The present MAP paradigm provides a completely different approach to the selection of the characteristics of the spatial decay of the atomic states: for each (sub)shell a single parameter provides a definite physical sense — a great intellectual and technical advantage of the proposed approach. So far implemented for the orbitals occupied in the ground state as treated in the Hartree-Fock setting, the MAP approach may be extended to excited (unoccupied in the ground state) atomic orbitals to formation of hierarchical basis sets as prescribed in Ref. 26. Indeed, adding further and further subshells entering with corresponding exponents with assured orthogonality eventually produces the required hierarchy of approximations.

This still needs to be controlled for convergence properties as well as tested for reasonable sources of the additional exponents for the subshells missing in the ground state. We will address this issue in a future work.

Although, maybe not well suitable for describing subtle physical effects depending on the details of the function behavior in the vicinity of the nucleus like magnetic properties and/or electric (hyper)polarizabilities, the very reasonable exponential decay at larger distances from the nuclei, important for bond formations and chemical reactivity, makes the MAP states a good alternative for studying chemistry. The paradigm may be extended as well to ionic states, and thus charge-transfer and ionic compounds. Instead of density plots expanded in a large number of Gaussian basis functions, a few orbital exponents may be

sufficient to characterize different chemical situations.

## III. CONCLUSIONS

By the present work, we continue our studies on minimally parameterized atomic states extending them either in terms of rows covered of the Mendeleev Periodic Table. We concentrate particularly on the spatial behavior of the MAP states as compared to that of the traditional Slater orbitals, refined Bunge and typical *ab initio* Gaussian atomic states. It turns out that the MAP states, although, showing much weaker oscillation amplitudes at the shorter electron-nucleus separations, manifest very large (typically more than 0.95) overlaps with the Bunge states on account of the almost coinciding positions of the radial nodes of the either series of orbitals. At the same time the similarity of the MAP states with the Slater orbitals allows to qualify the former as minimally orthogonalized Slater orbitals. In this quality the MAP states are perspective for developing new semi-empirical methods which habitually use the Slater basis sets which due to lack of the radial nodes cannot assure correct relative positioning of the states of the same $n$ but different $\ell$ on the energy scale. These and other issues and perspectives will be addressed in future work.

Additionally, we propose a numerical tool for comparing the relative quality of the basis sets through the Frobenius inner product of the operator (matrices) projecting to the subspaces spanned by the basis sets to be compared.

**Acknowledgments**

Calculations have been performed mainly in Paris, with the support of the research federation IP2CT to which P.R. wishes to express his gratitude.

---

[1] *P. Reinhardt, I.V. Popov, A.L. Tchougréeff*, "Minimum Atomic Parameter basis sets for elements 1 to 54 in a Hartree-Fock setting", Int.J.Quant.Chem. (Submitted/Previous paper in this issue)

[2] *I.V. Popov, A.L. Tchougréeff*, "Atomic orbitals revisited: generalized Hydrogen-like basis sets for 2$^{\text{nd}}$ row elements", Theor.Chem.Acc. **138** (2019) 9.

[3] *V.A. Fock, M.J. Petrashen*, "On the Numerical Solution of Generalized Equations of the Self-consistent Field", J.Exp.Theor.Phys. **4** (1934) 295 – 325 (engl. version: Phys.Zs.Sowj. **6**(1934) 368)

[4] *J.C. Slater*, "Quantum Theory of Atomic Structure", Vol 1, McGraw Hill, 1960

[5] *C.C.J. Roothaan, P.S. Bagus*, "", Methods in Comp.Phys. **2** (1963) 47

[6] *G. Malli*, Technical Report University of Chicago, Dpt Physics, Lab. of Mol. Struc. and Spectra, 1962/62 Part 2, pages 258-289 available at: `https://digital.library.unt.edu/ark:/67531/metadc228325/m1/`

[7] *C. Froese-Fischer*, "The Hartree-Fock Method for Atoms: A Numerical Approach", Wiley Intersciences, New York (1977)

[8] *M. Cinal*, "Highly accurate numerical solution of Hartree?Fock equation with pseudospectral method for closed-shell atoms", J.Math.Chem. **58** (2020) 1571–1600

[9] *C.F. Bunge, J.A. Barrientos, A.V. Bunge*, "", At.Data Nucl. Data Tables **53** (1993) 113 – 162

[10] *E. Madelung*, "Die Mathematischen Hilfsmittel des Physikers", 6. revidierte Auflage. Springer-Verlag, Berlin, Goettingen, Heidelberg (1957)

[11] *V.M. Klechkovsky*, "", Zh. Experim. i Teor. Fiz. **41** (1962) 465

[12] *C. Zener*, "Analytic Atomic Wave Functions", Phys.Rev. **36** (1930) 51

[13] *J.C. Slater*, "Atomic Shielding Constants", Phys.Rev. **36** (1930) 57

[14] *B. Pittel, W.H.E. Schwarz*, "Correlation energies from pseudo-potential calculations", Chem.Phys.Lett. **46** (1977) 121 https://doi.org/10.1016/0009-2614(77)85176-2

[15] *C. Teichteil, J.P. Malrieu, J.C. Barthelat*, "Non-empirical pseudopotentials for molecular calculations II. Basis set extension and correlation effects on the $X_2$ molecules (X=F, Cl, Br, I)", Mol.Phys. **33** (1977) 181 https://doi.org/10.1080/00268977700103151

[16] *M. Dolg*, "Valence correlation energies in pseudopotential calculations", Chem.Phys.Lett. **250** (1996) 75; *M. Dolg*, "On the accuracy of valence correlation energies in pseudopotential calculations", J.Chem.Phys. **104** (1996) 4061

[17] *P. Schwerdtfeger, B. Assadollahzadeh, U. Rohrmann, R. Schäfer, J.R. Cheeseman*, "Breakdown of the pseudopotential approximation for magnetizabilities and electric multipole moments: Test calculations for Au, AuF, and $Sn_n$ cluster ($n \leq 20$)", J.Chem.Phys. **134** (2011) 204102

[18] *Wolfram Research, Inc.*, "Mathematica", Champaign, IL, U.S.A. **Version 12.1,** (2020)

[19] *T. Kato*, "On the eigenfunctions of many-particle systems in quantum mechanics", Comm.Pure

Appl.Math. **10** (1957) 151–177

[20] *B. Nagy, F. Jensen*, "Basis sets in quantum chemistry", in Reviews in Computational Chemistry, A.L. Parrill, K.B. Lipkowitz Eds **30** (2017) 93 –149

[21] *W.J. Hehre, R.F. Stewart, J.A. Pople*, "Self-Consistent Molecular-Orbital Methods. I. Use of Gaussian Expansions of Slater-Type Atomic Orbitals", J.Chem.Phys. **51** (1969) 2657

[22] *R.D. Bardo, K. Ruedenberg*, "Even-Tempered Atomic Orbitals. 6. Optimal Orbital Exponents and Optimal Contractions of Gaussian Primitives for Hydrogen, Carbon, and Oxygen in Molecules", J.Chem.Phys. **60** (1974) 918

[23] *M.W. Schmidt, K. Ruedenberg*, "Effective Convergence to Complete Orbital Bases and to the Atomic Hartree-Fock Limit through Systematic Sequences of Gaussian Primitives", J.Chem.Phys. **71** (1979) 3951

[24] *E. Clementi, G. Corongiu*, "Geometrical basis set for molecular computations", Chem.Phys.Lett. **90** (1982) 359-363 https://doi.org/10.1016/0009-2614(82)83069-8

[25] *S. Huzinaga, M. Klobukowski, H. Tatewaki*, "The well-tempered GTF basis sets and their applications in the SCF calculations on N„ CO, $Na_2$, and $P_2$", Can.J.Chem. **63** (1985) 1812

[26] *V. Blum, R. Gehrke, F. Hanke, P. Havu, V. Havu, X. Ren, K. Reuter, M. Scheffler*, "Ab initio molecular simulations with numeric atom-centered orbitals", Comp.Phys.Comm. **180** (2009) 2175– 2196

## Appendix

### A. The Frobenius inner product

Given a basis of the Hilbert space of $L^2$ integrable functions we may define the projectors on the subspaces given by two (finite) orthonormal sets of atomic orbitals, as $\hat{M} = \sum_{\mu=1}^{m} |\mu\rangle\langle\mu|$ and $\hat{B} = \sum_{\beta=1}^{b} |\beta\rangle\langle\beta|$, respectively. The trace of the product of the two matrices $\mathrm{tr}(C^\dagger D)$ defines a scalar product (inner Frobenius product) in the space of matrices for which the usual matrix multiplication is possible, making the latter an Euclidean vector space. It has all properties of a scalar product — bilinearity and positive definiteness for $C = D$, but for $C$ being the zero matrix. Applying it to the square (projector) matrices $(M)_{\lambda\kappa} = \langle\lambda|\hat{M}|\kappa\rangle$ and $B$ yields:

$$
\begin{aligned}
\mathrm{tr}(M^\dagger B) &= \sum_{\kappa\lambda}\sum_{\mu}\sum_{\beta} \langle\kappa|\,\mu\rangle\langle\mu\,|\lambda\rangle\,\langle\lambda|\,\beta\rangle\langle\beta\,|\kappa\rangle \\
&= \sum_{\mu}\sum_{\beta}\langle\beta\underbrace{\sum_{\kappa}|\kappa\rangle\,\langle\kappa|}_{=\hat{1}}\,\mu\rangle\langle\mu\underbrace{\sum_{\lambda}|\lambda\rangle\,\langle\lambda|}_{=\hat{1}}\,\beta\rangle \\
&= \sum_{\mu}\sum_{\beta}\left|\langle\beta|\mu\rangle\right|^2 \quad ,
\end{aligned} \tag{3}
$$

where $|\lambda\rangle$ and $|\kappa\rangle$ run over a complete orthonormal basis in $\mathrm{L}^2$. That matrix elements are squared in the above expression does not destroy the bilinearity of the scalar product, as the underlying space is not the orbital space, but the space of the matrices acting in the Hilbert space.

A norm is derived as usual as the square root of the Frobenius inner product of a matrix with itself: $|C| = \sqrt{\mathrm{tr}(C^\dagger C)}$ and is known as the Frobenius matrix norm. The angle between two orbital subspaces is defined via its cosine as:

$$
\cos\varphi_F = \frac{\mathrm{tr}(M^\dagger B)}{|M|\;|B|} = \frac{\sum_{\mu=1}^{m}\sum_{\beta=1}^{b}\left|\langle\beta|\mu\rangle\right|^2}{\sqrt{m}\sqrt{b}} \quad . \tag{4}
$$

As the involved orbital sets (MAP and Bunge in the present case) are orthonormal, the inner product of either projector with itself is just the dimensionality of the subspaces $m$ or $b$ (number of elements in the respective orbital set, taking into account the multiplicity of $2\ell+1$ for a subshell with the azimuthal quantum number $\ell$) and the Frobenius norm is the square root of it. The expression eq. (4) is always non-negative, and falls between 0 and 1. It can be connected to the notion of a probability.

### B. Integration of energy contributions

For integrating one-electron contributions to the total energy it is sufficient to look at the radial functions. For the kinetic energy the radial part of the Laplace operator reads

$$
\frac{d^2}{dr^2} + \frac{2}{r}\frac{d}{dr} - \frac{\ell(\ell+1)}{r^2}
$$

which yields for a pair of primitive, unnormalized Slater functions for a given $\ell$

$$
\begin{aligned}
r^{(m-1)}e^{-\beta r}\,\Delta_r r^{(n-1)}e^{-\alpha r} &= r^{(m-1)}e^{-\beta r}\left(\frac{d^2}{dr^2} + \frac{2}{r}\frac{d}{dr} - \frac{\ell(\ell+1)}{r^2}\right) r^{(n-1)}e^{-\alpha r} \\
&= e^{-(\alpha+\beta)r}r^{(m+n-2)}\left(\frac{n(n-1)-\ell(\ell+1)}{r^2} + \alpha^2 - \frac{2}{r}n\alpha\right)
\end{aligned} \tag{5}
$$

For obtaining the kinetic energy density we have to multiply this with $-1/2$. We may notice that for instance for $\ell = n-1$ the density of the kinetic energy becomes negative for $r > (2n)/\alpha$.

Integrating a product of unnormalized Slater functions from 0 to $R$ gives

$$\int_0^R r^{(m-1)} e^{-\beta r} r^{(n-1)} e^{-\alpha r} r^2 dr = \int_0^R r^{(m+n)} e^{-(\alpha+\beta)r}\, dr =$$
$$= \left(\frac{1}{\alpha+\beta}\right)^{m+n+1} \left( (m+n)! - \underbrace{\Gamma(m+n+1, R(\alpha+\beta))}_{\to 0 \text{ for } R\to\infty} \right) \tag{6}$$

For the potential we find thus

$$\int_0^R r^{(m+n-1)} e^{-(\alpha+\beta)r}\, dr = \left(\frac{1}{\alpha+\beta}\right)^{m+n} \left( (m+n-1)! - \underbrace{\Gamma(m+n, R(\alpha+\beta))}_{\to 0 \text{ for } R\to\infty} \right) \tag{7}$$

$\Gamma(a,z) = \int_z^\infty t^{(a-1)} e^{-t}\, dt$ is the incomplete $\Gamma$ function for which routines exist to calculate its value to high precision.

We may recall that the normalized Slater function $S_n^\alpha(r)$ is

$$S_n^\alpha(r) = \frac{(2\alpha)^{3/2}}{\sqrt{\Gamma(2n+1)}}\, (2\,\alpha\, r)^{n-1}\, e^{-\alpha r} \tag{8}$$

For the radial integration of the kinetic energy the expressions become slightly more complicated:

$$\begin{aligned}
&-\frac{1}{2}\int_0^R S_m^\beta(r) \left( \frac{d^2}{dr^2} + \frac{2}{r}\frac{d}{dr} - \frac{\ell(\ell+1)}{r^2} \right) S_n^\alpha(r) r^2 dr \\
&= \frac{2^{m-1}\beta^{m+1/2}}{\sqrt{mn\Gamma(2m)\Gamma(2n)}} \times \left( -\frac{2^n n(n-1)\alpha^{n+3/2}(m+n-2)!}{(\alpha+\beta)^{m+n}} + \right. \\
&\frac{\ell(\ell+1)}{\beta^m}\sqrt{n\Gamma(2n)} \left( \Gamma(m) - \underbrace{\Gamma(m, R\beta)}_{\to 0 \text{ for } R\to\infty} \right) - \\
&\frac{2^n e^{-R(\alpha+\beta)} \alpha^{n+1/2} R^{m+n-1} (n(n-1)(\alpha+\beta) - (m+n-1)R\alpha^2)}{(m+n-1)\ (\alpha+\beta)} + \\
&\frac{2^n \alpha^{n+1/2}}{(m+n-1)\ (\alpha+\beta)^{m+n+1}} \times \\
&\left\{ \left( (m-m^2)\alpha^2 + 2mn\beta + n(n-1)(\alpha^2+\alpha\beta-\beta^2) \right) (m+n-1)! + \right. \\
&\left. \left. \underbrace{\left( m(m-1)\alpha^2 - 2mn\alpha\beta + n(n-1)\beta^2 \right) \Gamma(m+n, R(\alpha+\beta))}_{\to 0 \text{ for } R\to\infty} \right\} \right)
\end{aligned} \tag{9}$$

For $R \to \infty$ we are left with

$$
\begin{aligned}
& -\frac{1}{2}\int_0^\infty r^{(m-1)}e^{-\beta r}\left(\frac{d^2}{dr^2}+\frac{2}{r}\frac{d}{dr}-\frac{\ell(\ell+1)}{r^2}\right)r^{(n-1)}e^{-\alpha r}r^2dr \\
= \; & \frac{2^{m-1}\beta^{m+1/2}}{\sqrt{mn\Gamma(2m)\Gamma(2n)}}\times\left(-\frac{2^n n(n-1)\alpha^{n+3/2}(m+n-2)!}{(\alpha+\beta)^{m+n}}+\right. \\
& \frac{\ell(\ell+1)}{\beta^m}\sqrt{n\Gamma(2n)}\Gamma(m)+\frac{2^n\alpha^{n+1/2}}{(\alpha+\beta)^{m+n+1}}\times \\
& \left.\left((m-m^2)\alpha^2+2mn\beta+n(n-1)(\alpha^2+\alpha\beta-\beta^2)\right)(m+n-2)!\right) \qquad (10) \\
= \; & \frac{2^{m-1}\sqrt{\beta}\;(m-1)!}{\sqrt{m\,(2m-1)!}}\ell(\ell+1)-\frac{2^{m+n-1}\alpha^{n+1/2}\beta^{m+1/2}}{\sqrt{mn\Gamma(2m)\Gamma(2n)}(\alpha+\beta)^{m+n+1}}(m+n-2)!\times \\
& \left((m-m^2)\alpha^2+2mn\beta+n(n-1)(\alpha^2+\alpha\beta-\beta^2)-n(n-1)\alpha(\alpha+\beta)\right) \qquad (11) \\
= \; & \frac{2^{m-1}\sqrt{\beta}\;(m-1)!}{\sqrt{m\,(2m-1)!}}\ell(\ell+1)- \\
& \frac{2^{m+n-1}\alpha^{n+1/2}\beta^{m+1/2}\,(m(m-1)\alpha^2-2mn\beta+n(n-1)\beta^2)}{\sqrt{mn\Gamma(2m)\Gamma(2n)}(\alpha+\beta)^{m+n+1}}(m+n-2)! \qquad (12)
\end{aligned}
$$

Mathematica gives for the latter the same two terms.